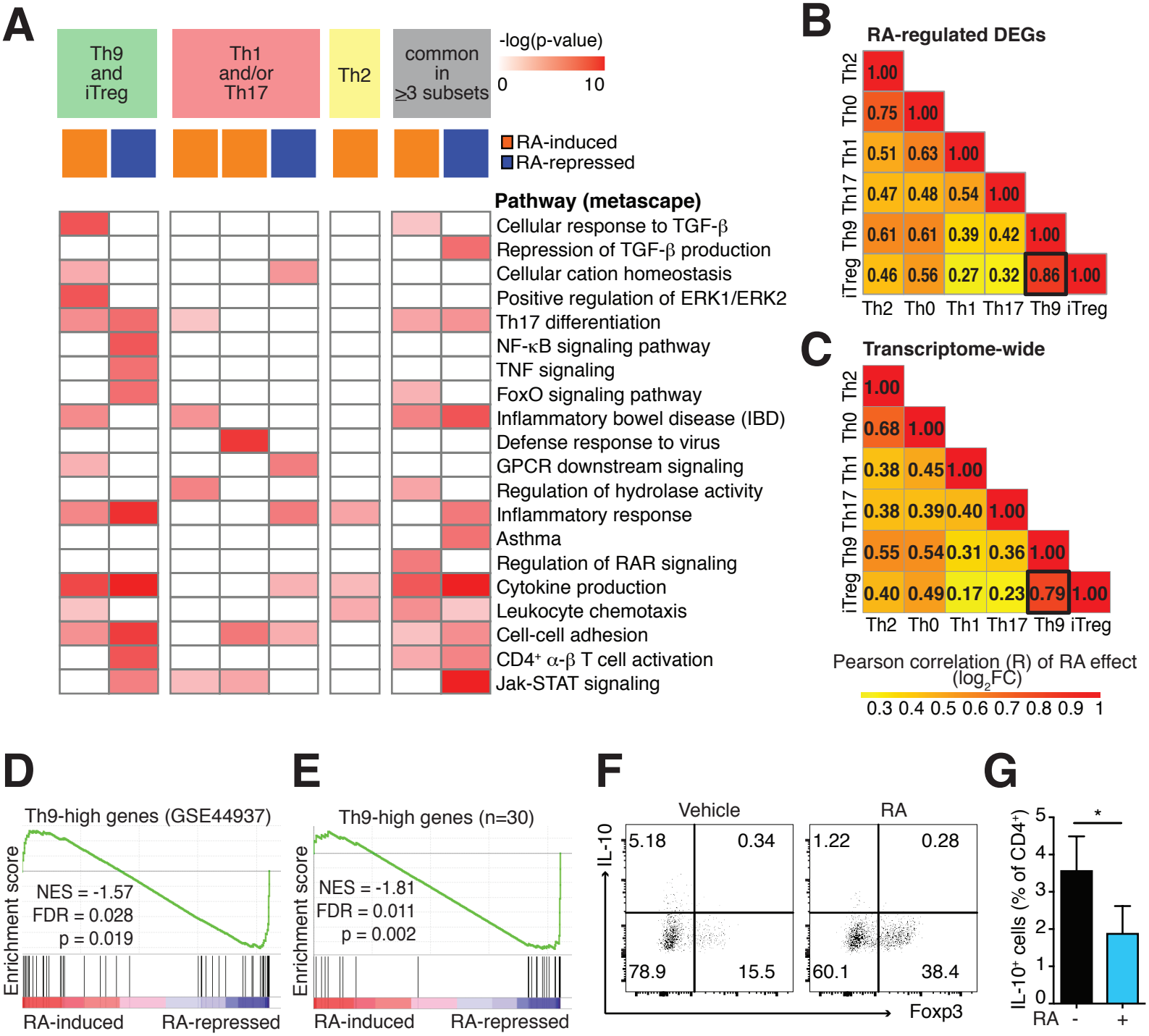

Figure S1, related to Figure 1-3. A. Metascape pathway analysis of RA-regulated modules. -log(p-values) are shown for pathways enriched in each module. **B,C. Correlation plots showing regression analysis of RA effect in T cells**. Pearson's correlation (R) was calculated for RA effect (log_2 normalized fold-change in gene expression, RA vs. vehicle control) of 1025 RA-regulated genes. High R value indicates a similar effect. Data are shown for RA-regulated differentially expressed genes, or DEGs (B) and transcriptome-wide (C). **D. RA effect on Th9-high genes, Gene Set Enrichment Analysis (GSEA).** Gene Set Enrichment Analysis (GSEA) plot depicts effect of RA on the entire Th9-high geneset, accounting for the net, or average, effect on all the genes in the geneset. **E. RA effect on an independently generated Th9-high geneset, GSEA.** A list of Th9-high genes was generated using a public dataset that contained gene expression data on Th9, Th2, and iTreg cells (GSE44973). GSEA plot depicts the effect of RA on the average, or net, expression of genes in this geneset. **F,G. Flow cytometric analysis of IL-10 vs. Foxp3 expression Th9 cells differentiated in the presence of vehicle control or RA 1000nM.** F. Representative flow cytometric plots showing IL-10 vs. Foxp3 expression. G. Bar graphs summarizing IL-10 expression (Data are shown as mean ± SEM; n=6; *p<0.05 paired t-test)

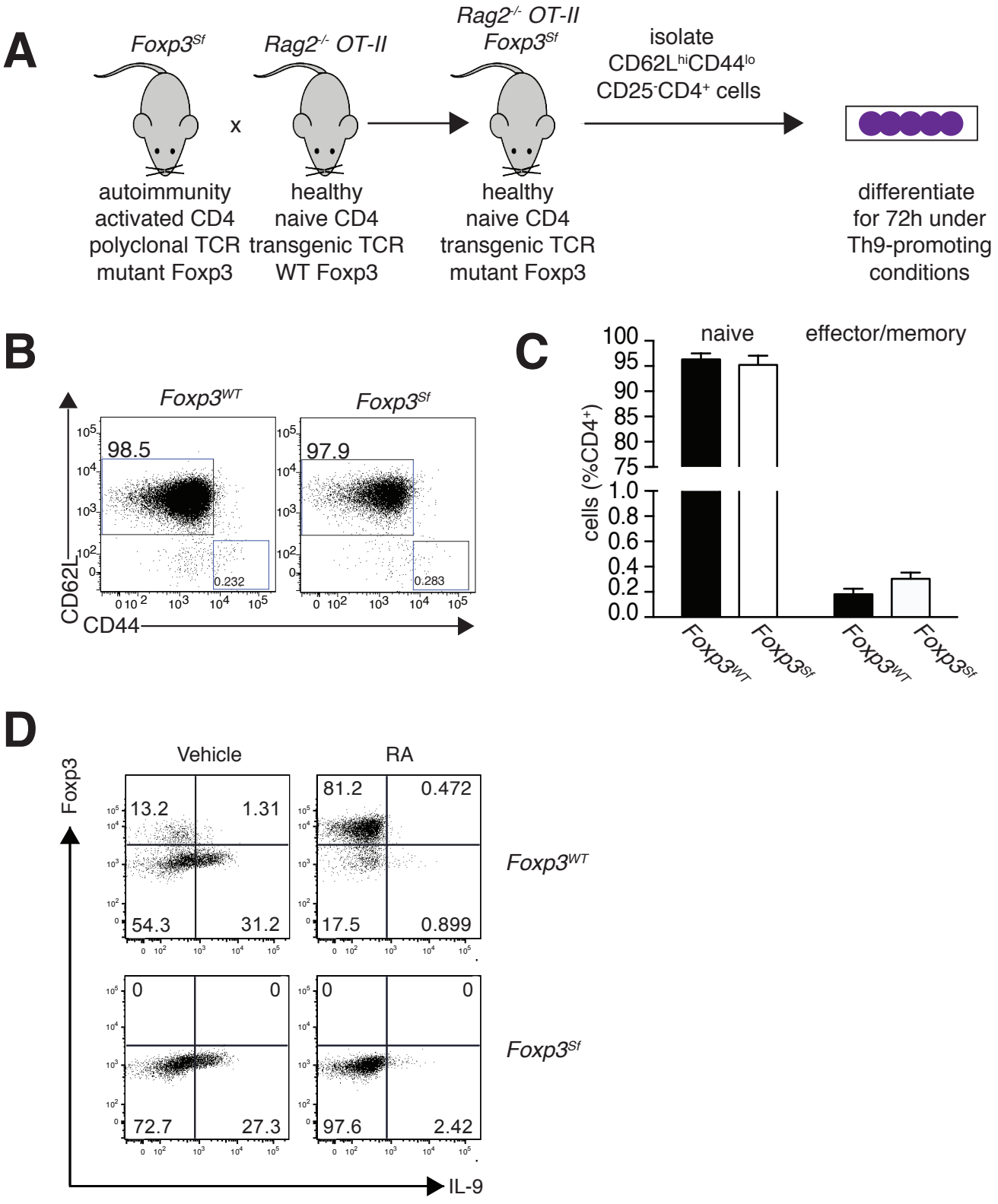

Figure S2, related to Figure 4. A. Generation of *Rag2*$^{-/-}$ *OT-II Foxp3*^{Sf} mice. Mice carrying the *Foxp3*^{Sf} (Scurfy) mutation were crossed to *Rag2*$^{-/-}$ *OT-II* mice to generate *Rag2*$^{-/-}$ *OT-II Foxp3*^{Sf} mice. CD4^{+} T cells from *Rag2*$^{-/-}$ *OT-II Foxp3*^{Sf} (denoted *Foxp3*^{Sf}) and *Rag2*$^{-/-}$ *OT-II Foxp3*^{WT} mice(denoted *Foxp3*^{WT}) were compared. Naïve (CD62L^{hi}/CD44^{lo}/CD25^{-}/CD4^{+}) T cells were isolated and cultured in vitro for 72 hours under Th9-promoting conditions with either vehicle control or 1000 nM RA. **B-C. Flow cytometric analysis of naïve and effector/memory cell surface markers in CD4^{+} T cells from *Foxp3*^{WT} and *Foxp3*^{Sf} mice.** B. Representative flow cytometric plots show CD62L and CD44 expression in *Foxp3*^{WT} and *Foxp3*^{Sf} CD4^{+} T cells. C. Bar graphs summarize CD62L and CD44 expression in *Foxp3*^{WT} and *Foxp3*^{Sf} CD4^{+} T cells (Data are shown as mean ± SEM; n=4) **D. Representative flow cytometric plot showing IL-9 vs. Foxp3 expression in *Foxp3*^{WT} and *Foxp3*^{Sf} Th9 cells.**

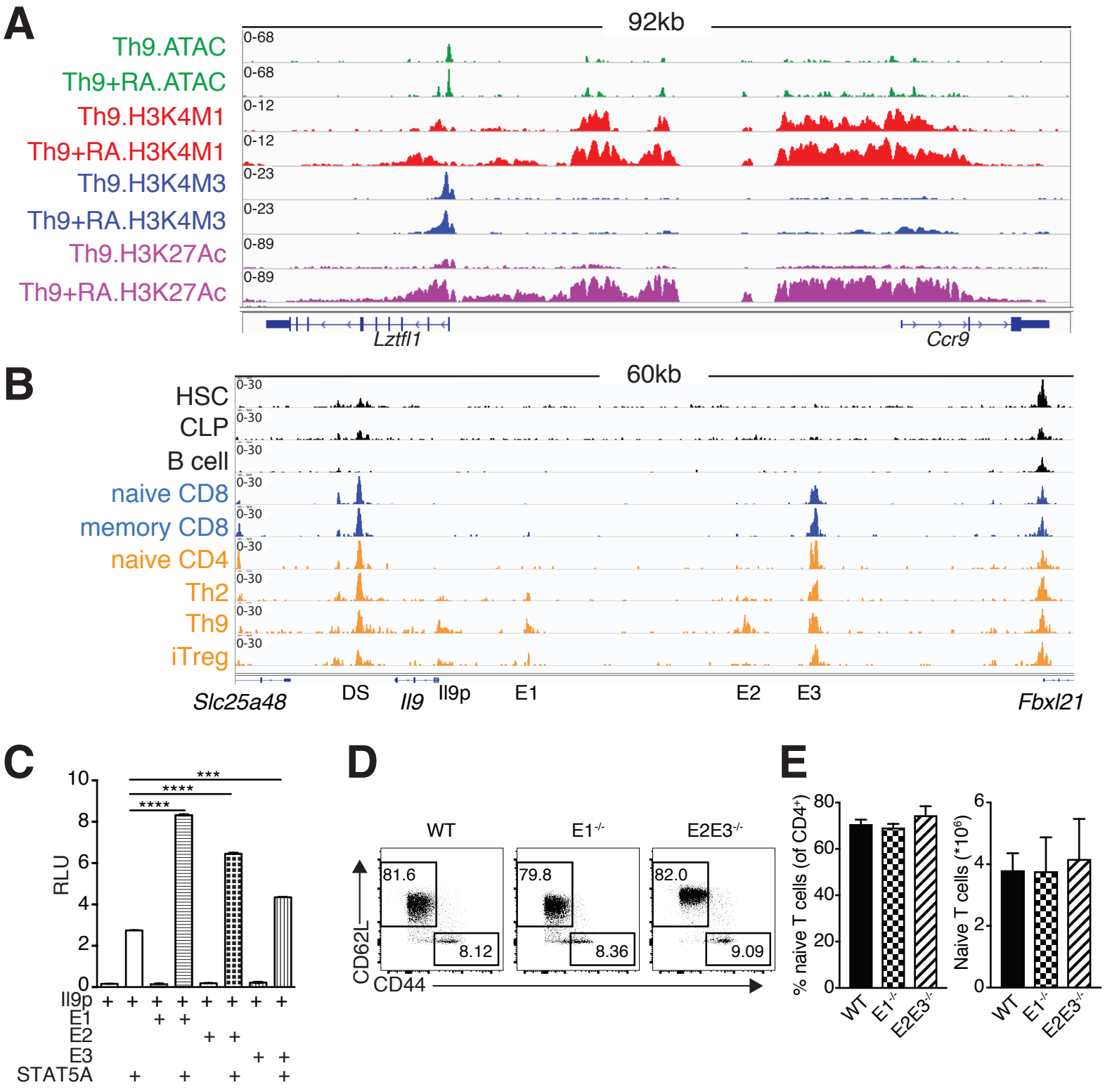

Figure S3, related to Figure 5. A. *Ccr9* regulatory elements identified by histone modifications and chromatin accessibility, and RA effect on regulatory elements. *Ccr9* gene tracks of ATAC, H3K4M1, H3K4M3, and H3K27Ac in Th9 cells polarized in the presence of vehicle control or 1000 nM RA. **B. *Il9* regulatory elements identified by chromatin accessibility in multiple cell types**. *Il9* gene tracks showing ATAC peaks in four CD4$^+$ T cell subsets (yellow), hematopoietic stem cells (HSC), common lymphoid progenitors (CLP), B cells, and CD8$^+$ T cells. Data from Th2, naive CD4$^+$ T cells, CD8$^+$ T cells, HSC, and CLP were obtained from public data (GSE77695). **C. Luciferase enhancer assay testing Il9 regulatory elements E1-E3.** The Il9 promoter was cloned either alone or in tandem with E1, E2, or E3 into the luciferase reporter vector pGL4.23. HEK293T cells were cotransfected with each construct and constitutively active Stat5A (n=4, ***p<0.005,****p<0.001, unpaired t-test). **D-E. Flow cytometric analysis of naïve and memory cell surface markers in CD4$^+$ T cells from E1$^{-/-}$ and E2E3$^{-/-}$ mice.** D. Representative flow cytometric plots show CD62L and CD44 expression in CD4$^+$ T cells isolated from spleen and lymph nodes of WT, E1$^{-/-}$, and E2E3$^{-/-}$ mice. E. Bar graphs summarize percentages and absolute numbers of naïve (CD62L$^+$ CD25$^-$ CD44^{lo}) CD4$^+$ T cells from WT, E1$^{-/-}$, and E2E3$^{-/-}$ mice. Data are shown as mean ± SEM; n=3-4

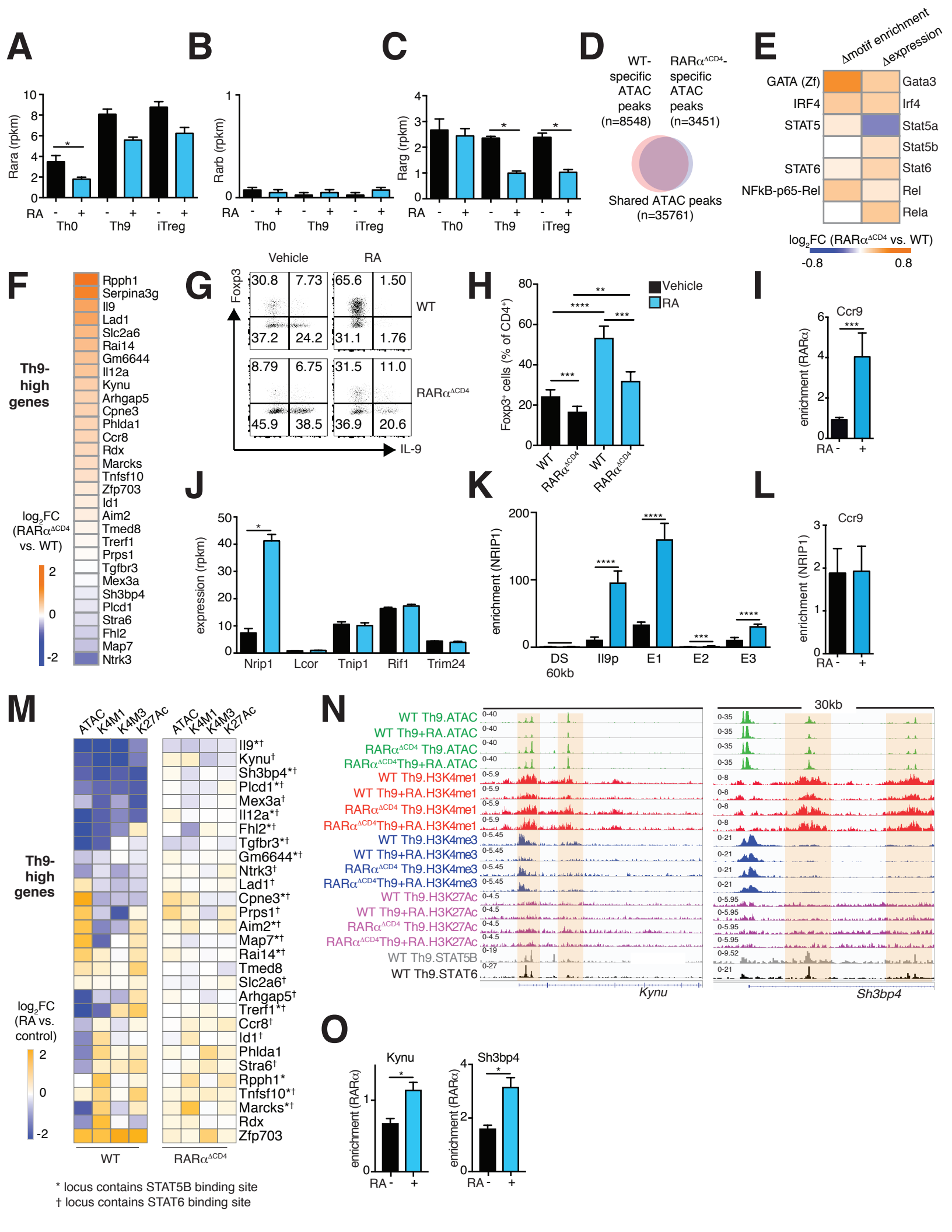
A
Rara (rpkm)
RA
Th0
Th9
iTreg
B
Rarb (rpkm)
C
Rarg (rpkm)
D
WT-specific ATAC peaks (n=8548)
RARα^ΔCD4-specific ATAC peaks (n=3451)
Shared ATAC peaks (n=35761)
E
Δmotif enrichment
Δexpression
GATA (Zf)
IRF4
STAT5
STAT6
NFkB-p65-Rel
Gata3
Irf4
Stat5a
Stat5b
Stat6
Rel
Rela
log2FC (RARα^ΔCD4 vs. WT)
-0.8
0.8
F
Th9-high genes
Rpph1
Serpina3g
Il9
Lad1
Slc2a6
Rai14
Gm6644
Il12a
Kynu
Arhgap5
Cpne3
Phlda1
Ccr8
Rdx
Marcks
Tnfsf10
Zfp703
Id1
Aim2
Tmed8
Trerf1
Prps1
Tgfbr3
Mex3a
Sh3bp4
Plcd1
Stra6
Fhl2
Map7
Ntrk3
log2FC (RARα^ΔCD4 vs. WT)
G
Vehicle
RA
Foxp3
IL-9
WT
RARα^ΔCD4
30.8
7.73
37.2
24.2
65.6
1.50
31.1
1.76
8.79
6.75
45.9
38.5
31.5
11.0
36.9
20.6
H
Foxp3+ cells (% of CD4+)
Vehicle
RA
WT
RARα^ΔCD4
I
Ccr9
enrichment (RARα)
RA
J
expression (rpkm)
Nrip1
Lcor
Tnip1
Rif1
Trim24
K
enrichment (NRIP1)
DS 60kb
Il9p
E1
E2
E3
L
Ccr9
enrichment (NRIP1)
M
ATAC
K4M1
K4M3
K27Ac
Th9-high genes
Il9*†
Kynu†
Sh3bp4*†
Plcd1*†
Mex3a†
Il12a*†
Fhl2*†
Tgfbr3*†
Gm6644*†
Ntrk3†
Lad1†
Cpne3*†
Prps1†
Aim2*†
Map7*†
Rai14*†
Tmed8
Slc2a6†
Arhgap5†
Trerf1*†
Ccr8†
Id1†
Phlda1
Stra6†
Rpph1*
Tnfsf10*†
Marcks*†
Rdx
Zfp703
log2FC (RA vs. control)
WT
RARα^ΔCD4
* locus contains STAT5B binding site
† locus contains STAT6 binding site
N
WT Th9.ATAC
WT Th9+RA.ATAC
RARα^ΔCD4 Th9.ATAC
RARα^ΔCD4Th9+RA.ATAC
WT Th9.H3K4me1
WT Th9+RA.H3K4me1
RARα^ΔCD4 Th9.H3K4me1
RARα^ΔCD4Th9+RA.H3K4me1
WT Th9.H3K4me3
WT Th9+RA.H3K4me3
RARα^ΔCD4 Th9.H3K4me3
RARα^ΔCD4Th9+RA.H3K4me3
WT Th9.H3K27Ac
WT Th9+RA.H3K27Ac
RARα^ΔCD4 Th9.H3K27Ac
RARα^ΔCD4Th9+RA.H3K27Ac
WT Th9.STAT5B
WT Th9.STAT6
Kynu
30kb
Sh3bp4
O
Kynu
Sh3bp4
enrichment (RARα)
RA

Figure S4. Related to Figure 6. A-C. *Rara , Rarb*, and *Rarg* expression in three different Th subsets treated with vehicle control or RA. Bar graphs summarize expression values (reads per kilobase of transcript per million mapped reads, or rpkm) of *Rara, Rarb,* and *Rarg* from RNA-sequencing (n=2, *FDR<0.05). **D,E. TFs with RARα-regulated motif accessibility and RARα-regulated gene expression.** Venn diagram (D) shows changes in global genomic accessibility (number of ATAC peaks gained and lost) with RARα deletion in Th9 conditions. Heatmap (E) displays RARα effect on motif enrichment and gene expression for Th9-promoting TFs. **F. Cell-intrinsic RARα effect on Th9-high genes in Th9 cells.** Heatmaps depict $\log_2$ normalized average fold change in gene expression (RARα$^{\Delta}$CD4 vs. WT, n=3) for Th9-high genes. **G,H. Foxp3 expression in WT vs. RARα$^{\Delta CD4}$ Th9 cells.** G. Representative flow cytometric plots of IL-9 vs. Foxp3 expression in cells cultured under Th9 conditions with vehicle control or 1000 nM RA. H. Bar graph summarizing Foxp3 expression (n=5). **p<0.01,***p<0.005,****p<0.001, paired t-test. **I. RARα binding at Ccr9 RA response element (RARE).** Binding enrichment (ChIP-qPCR) of RARα relative to input in cells cultured under Th9 conditions with RA or vehicle control. **J. RAR corepressor expression in Th9 cells.** Representative bar graphs display gene expression (rpkm) of five major RAR-associated corepressors in cells cultured under Th9 conditions in cells treated with vehicle control or RA. (n=2, *FDR<0.05) **K**. **ChIP-qPCR for NRIP1 at Il9 regulatory elements in Th9 cells treated with vehicle control or RA.** Bar graphs summarize binding enrichment for NRIP1 relative to input at the five Il9 regulatory elements. **L. NRIP1 binding at Ccr9 RARE.** Binding enrichment (ChIP-qPCR) of NRIP1 relative to input at Ccr9 regulatory elements in cells treated with vehicle control or RA. **M. Effect of RA on chromatin accessibility and histone modifications of regulatory elements associated with Th9-high genes, in WT and RARα$^{\Delta CD4}$ Th9 cells.** Heatmaps depict fold-change in accessibility (ATAC) or histone marks (H3K4M1, H3K4M3, K3K27Ac) at the most strongly RA-regulated peak (greatest fold-change in signal, RA vs. control) in WT and RARα$^{\Delta CD4}$ Th9 cells polarized in the presence of vehicle control or 1000 nM RA. Genes marked with * contain STAT5 binding sites, and genes marked with † contain STAT6 binding sites, within their extended loci. **N. Chromatin accessibility and histone modifications at the loci of representative RA-repressed Th9-high gene, STAT5 and STAT6 binding sites, and RA effect on the loci in WT and RARα$^{\Delta CD4}$ Th9 cells.** *Kynu* and *Sh3bp4* were chosen as representative genes based on similar RA-mediated epigenetic and transcriptional regulation to *Il9*. Gene tracks show ATAC, H3K4M1, H3K4M3, and H3K27Ac in WT and RARα$^{\Delta CD4}$ Th9 cells polarized in the presence of vehicle control or 1000 nM RA. Gene tracks also show STAT5B and STAT6 binding sites in Th9 cells based on public data (GSE41317). **O. RARα binding at the promoters of representative Th9-high genes.** Bar graphs show binding enrichment (ChIP-qPCR) of RARα relative to input at the *Kynu,* and *Sh3bp4* promoters in cells cultured under Th9 conditions in the presence of control. (For all ChIP-qPCR: n=3,*p<0.05,**p<0.01,***p<0.005,****p<0.001, unpaired t-test). All pooled data shown as mean ± SEM.

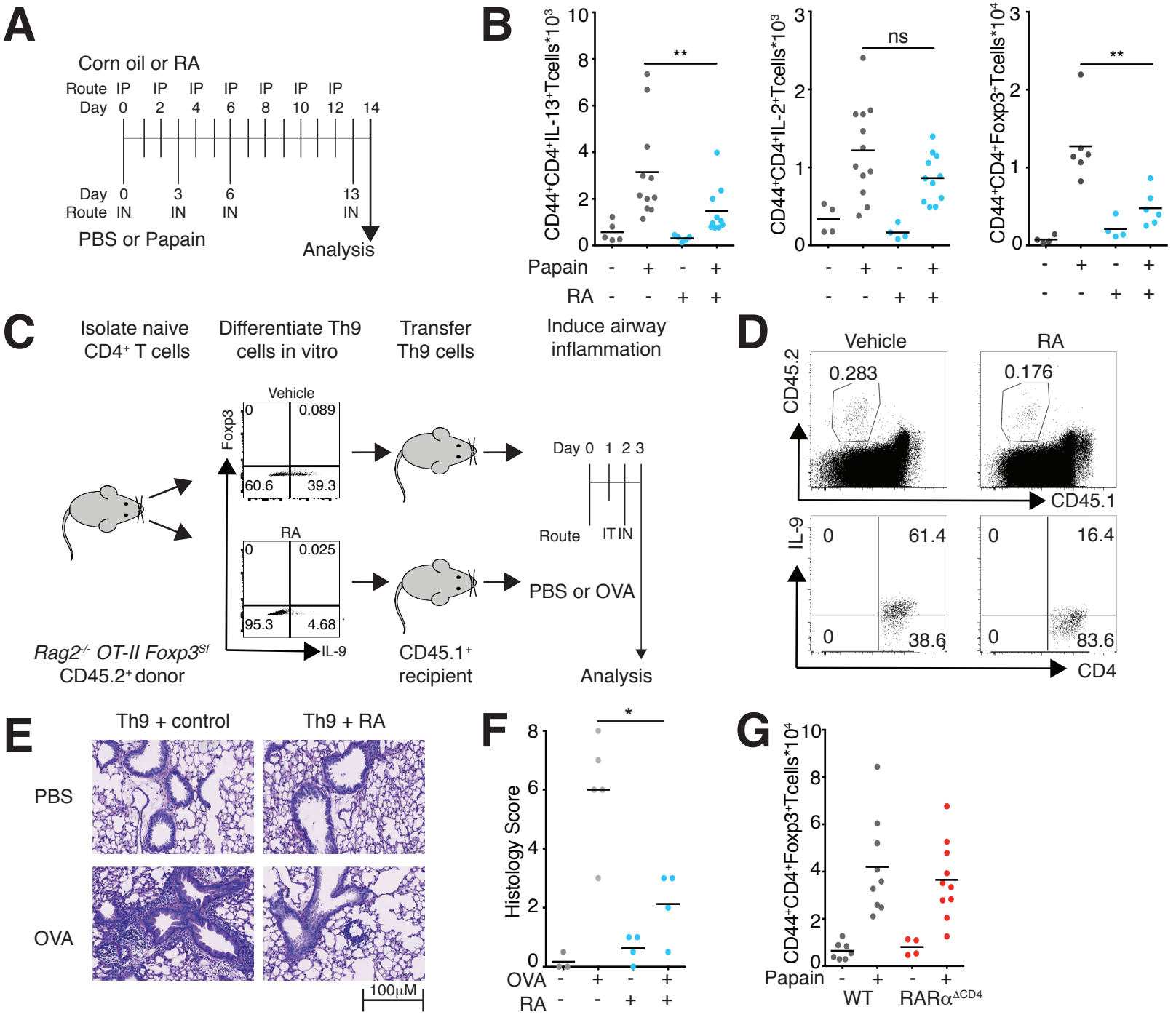

Figure S5, related to Figure 7. A. Experimental design of papain-induced chronic airway disease. Mice were exposed to serial intranasal injections of 25 μg papain on d0, 3, 6, and 13. For RA treatment experiments, mice were simultaneously treated with intraperitoneal injections of RA (treatment) or DMSO (control) in corn oil. **B. Flow cytometric analysis of IL-13$^+$, IL-2$^+$, and Foxp3$^+$ Lin$^-$TCRβ$^+$CD4$^+$CD44^{hi} cells in lung tissue of mice treated with vehicle control or RA, d14 papain-induced asthma**. Graphs show absolute numbers of Th cells that express IL-13, IL-2, and Foxp3. (1-2 replicates, n= 3-5 per replicate), *p<0.05,**p<0.01, Mann Whitney. **C. Experimental design of Th9 transfer experiment.** Naive CD4$^+$ T cells were isolated from *Rag2$^{-/-}$ OT-II Foxp3^{Sf}* CD45.2$^+$ mice and differentiated *in vitro* under Th9-promoting conditions in the presence of RA (1000nM) or vehicle control. After 72 hours, the Th9 cells were transferred intravenously to CD45.1$^+$ recipients. Mice were challenged 24 h after transfer intratracheally and 48 h after transfer intranasally with injections of ovalbumin (100μg). **D. Flow cytometric analysis of CD45.2$^+$ (donor) Lin$^-$TCRβ$^+$CD4$^+$IL-9$^+$ cells in lung tissue of CD45.1$^+$ (recipient) mice.** Representative flow cytometric plot reveals fewer IL-9$^+$ donor T cells in the recipient mice. **E,F. Lung inflammation in mice undergoing transfer with control-treated or RA-treated Th9 cells, after 3-day ovalbumin challenge.** E. Representative images of PAS stained slides demonstrate reduced lymphocytic infiltration in mice undergoing transfer with RA-treated vs. control-treated Th9 cells. F. Pulmonary histology scores in mice undergoing transfer with RA-treated or control-treated Th9 cells. (2 replicates, n= 1-3 per replicate); **p<0.01, Mann Whitney. **G. Flow cytometric analysis of Foxp3 expressing Lin$^-$TCRβ$^+$CD4$^+$CD44^{hi} cells in lung tissue of in WT or RARα^{ΔCD4} mice, d14 papain-induced asthma.** Graph shows absolute numbers of Th cells expressing Foxp3 (2 replicates, n=3-5 per replicate); *p<0.05,**p<0.01, Mann Whitney.

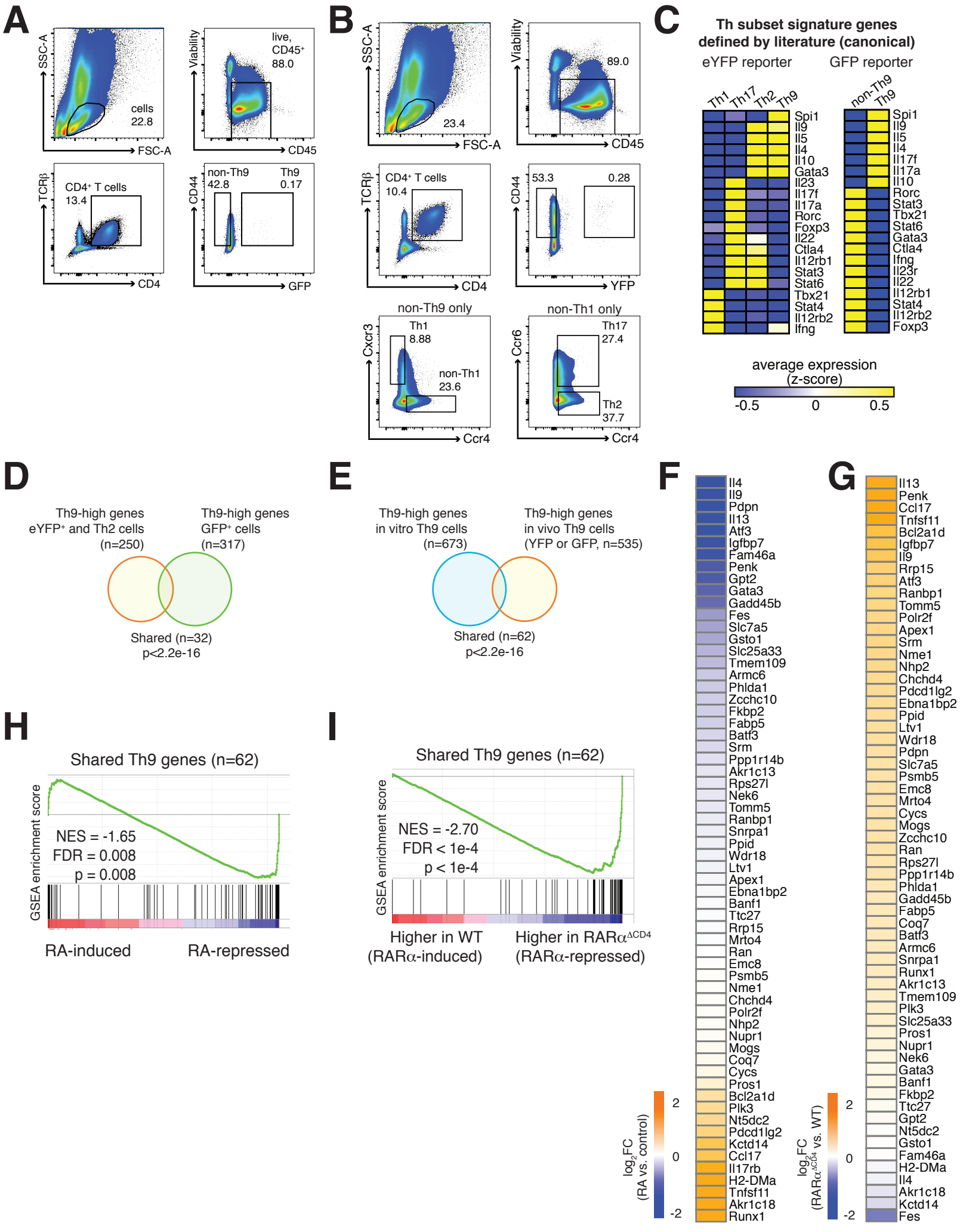
A
SSC-A
FSC-A
cells
22.8
Viability
CD45
live,
CD45+
88.0
TCRβ
CD4
CD4+ T cells
13.4
CD44
GFP
non-Th9
42.8
Th9
0.17
B
SSC-A
FSC-A
23.4
Viability
CD45
89.0
TCRβ
CD4
CD4+ T cells
10.4
CD44
YFP
53.3
0.28
non-Th9 only
Cxcr3
Ccr4
Th1
8.88
non-Th1
23.6
non-Th1 only
Ccr6
Ccr4
Th17
27.4
Th2
37.7
C
Th subset signature genes
defined by literature (canonical)
eYFP reporter
GFP reporter
Th1
Th17
Th2
Th9
non-Th9
Th9
Spi1
Il9
Il5
Il4
Il10
Gata3
Il23
Il17f
Il17a
Rorc
Foxp3
Il22
Ctla4
Il12rb1
Stat3
Stat6
Tbx21
Stat4
Il12rb2
Ifng
Il17f
Il17a
Il10
Rorc
Stat3
Tbx21
Stat6
Gata3
Ctla4
Ifng
Il23r
Il22
Il12rb1
Stat4
Il12rb2
Foxp3
average expression
(z-score)
-0.5
0
0.5
D
Th9-high genes
eYFP+ and Th2 cells
(n=250)
Th9-high genes
GFP+ cells
(n=317)
Shared (n=32)
p<2.2e-16
E
Th9-high genes
in vitro Th9 cells
(n=673)
Th9-high genes
in vivo Th9 cells
(YFP or GFP, n=535)
Shared (n=62)
p<2.2e-16
F
Il4
Il9
Pdpn
Il13
Atf3
Igfbp7
Fam46a
Penk
Gpt2
Gata3
Gadd45b
Fes
Slc7a5
Gsto1
Slc25a33
Tmem109
Armc6
Phlda1
Zcchc10
Fkbp2
Fabp5
Batf3
Srm
Ppp1r14b
Akr1c13
Rps27l
Nek6
Tomm5
Ranbp1
Snrpa1
Ppid
Wdr18
Ltv1
Apex1
Ebna1bp2
Banf1
Ttc27
Rrp15
Mrto4
Ran
Emc8
Psmb5
Nme1
Chchd4
Polr2f
Nhp2
Nupr1
Mogs
Coq7
Cycs
Pros1
Bcl2a1d
Plk3
Nt5dc2
Pdcd1lg2
Kctd14
Ccl17
Il17rb
H2-DMa
Tnfsf11
Akr1c18
Runx1
log2FC
(RA vs. control)
2
0
-2
G
Il13
Penk
Ccl17
Tnfsf11
Bcl2a1d
Igfbp7
Il9
Rrp15
Atf3
Ranbp1
Tomm5
Polr2f
Apex1
Srm
Nme1
Nhp2
Chchd4
Pdcd1lg2
Ebna1bp2
Ppid
Ltv1
Wdr18
Pdpn
Slc7a5
Psmb5
Emc8
Mrto4
Cycs
Mogs
Zcchc10
Ran
Rps27l
Ppp1r14b
Phlda1
Gadd45b
Fabp5
Coq7
Batf3
Armc6
Snrpa1
Runx1
Akr1c13
Tmem109
Plk3
Slc25a33
Pros1
Nupr1
Nek6
Gata3
Banf1
Fkbp2
Ttc27
Gpt2
Nt5dc2
Gsto1
Fam46a
H2-DMa
Il4
Akr1c18
Kctd14
Fes
log2FC
(RARα^ΔCD4 vs. WT)
2
0
-2
H
Shared Th9 genes (n=62)
GSEA enrichment score
NES = -1.65
FDR = 0.008
p = 0.008
RA-induced
RA-repressed
I
Shared Th9 genes (n=62)
GSEA enrichment score
NES = -2.70
FDR < 1e-4
p < 1e-4
Higher in WT
(RARα-induced)
Higher in RARα^ΔCD4
(RARα-repressed)

Figure S6, related to Figure 7. A,B. Sorting strategy for in vivo Th9 cells. Flow cytometric plots depict fluorescence-activated cell sorting (FACS) strategy from GFP IL-9 reporter mice (A) and eYFP IL-9 fate reporter mice (B). $CD4^+$ T cells from IL-9 fate reporter mice, cells were sorted based on eYFP expression. $eYFP^-$ cells were further sorted based on cell surface markers to either Th1 ($Cxcr3^+$, $Ccr4^-$), Th2 ($Cxcr3^-$, $Ccr4^+$, $Ccr6^-$), or Th17 ($Cxcr3^-$, $Ccr4^+$, $Ccr6^+$) subsets as comparator groups. $CD4^+$ T cells from IL-9 reporter mice were sorted based on GFP expression. **C. Expression of Th subset signature genes *in vivo* Th9 cells and other subsets.** Heatmaps depict average expression (reads per kilobase of transcript, or rpkm) normalized to mean expression of genes known to correlate with Th9 identity *in vivo* (*Il9, Spi1*) and of several known Th1, Th2, Th17, and Treg subset signature genes. **D. Overlap between in vivo Th9-high genes using two different models of IL-9 reporting.** Venn diagram depicts the number of differentially expressed (FDR<0.05, FC≥1.5, ANOVA) Th9-high genes (DEGs) defined by eYFP model (comparing IL9 expression $eYFP^+$ and Th2 cells vs. non Il9-expressing Th1 and Th17 cells, n=250) or GFP model (comparing GFP^+ vs. GFP^- cells, n=317), in vitro Th9 cells (blue, n=671), and overlap between the two (n=32, p<2.2e-16, Fisher's exact t-test). **E. Overlap between in vitro and in vivo Th9-high genes.** Venn diagram depicts the number of differentially expressed (average FC≥1.5, FDR<0.05, ANOVA) Th9-high genes (DEGs) defined by in vivo Th9 models (eYFP or GFP reporters, n=535), in vitro Th9 cells (blue, n=671), and overlap between the two (n=62, p<2.2e-16, Fisher's exact t-test). Shared Th9 genes were defined by overlap between in vitro and in vivo Th9-high genes. **F-I Shared Th9 genes and RA effect on these genes.** F. Heatmap depicts RA effect (log_2 average fold change in expression, RA vs. control) on expression of shared Th9 genes. G. Heatmap depicts effect effect of RARα deletion (log_2 average fold change in expression, $RAR\alpha^{\Delta CD4}$ vs. WT) on expression of shared Th9 genes. H,I. The effect of RA (H) and RARα (I) on the average, or net, expression of genes in this geneset was tested by GSEA.

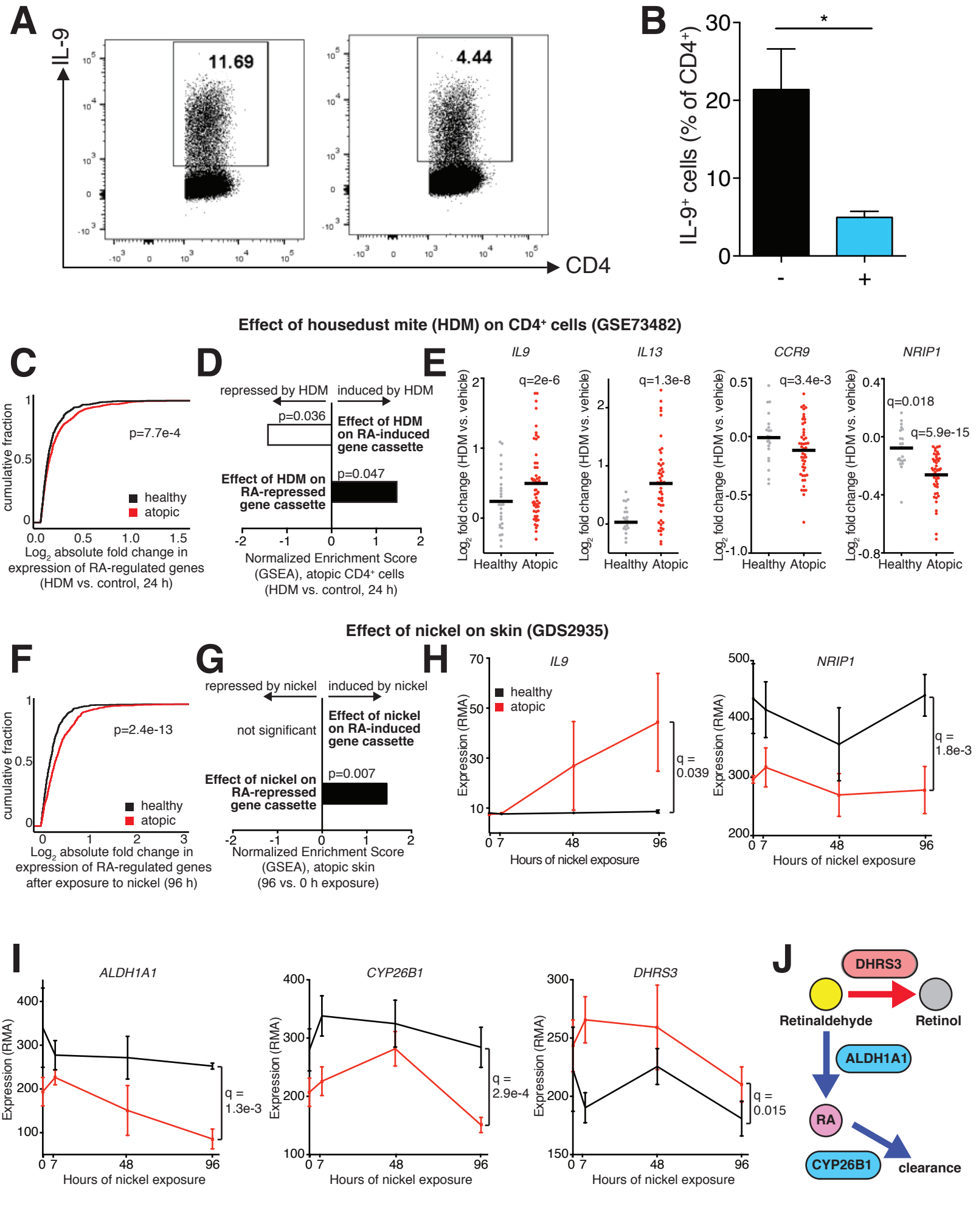
A
IL-9
CD4
11.69
4.44
B
IL-9+ cells (% of CD4+)
*
-
+
Effect of housedust mite (HDM) on CD4+ cells (GSE73482)
C
cumulative fraction
p=7.7e-4
healthy
atopic
Log2 absolute fold change in expression of RA-regulated genes (HDM vs. control, 24 h)
D
repressed by HDM
induced by HDM
p=0.036
Effect of HDM on RA-induced gene cassette
Effect of HDM on RA-repressed gene cassette
p=0.047
Normalized Enrichment Score (GSEA), atopic CD4+ cells (HDM vs. control, 24 h)
E
IL9
IL13
CCR9
NRIP1
q=2e-6
q=1.3e-8
q=3.4e-3
q=0.018
q=5.9e-15
Log2 fold change (HDM vs. vehicle)
Healthy
Atopic
Effect of nickel on skin (GDS2935)
F
cumulative fraction
p=2.4e-13
healthy
atopic
Log2 absolute fold change in expression of RA-regulated genes after exposure to nickel (96 h)
G
repressed by nickel
induced by nickel
not significant
Effect of nickel on RA-induced gene cassette
Effect of nickel on RA-repressed gene cassette
p=0.007
Normalized Enrichment Score (GSEA), atopic skin (96 vs. 0 h exposure)
H
IL9
NRIP1
Expression (RMA)
healthy
atopic
q = 0.039
q = 1.8e-3
Hours of nickel exposure
I
ALDH1A1
CYP26B1
DHRS3
q = 1.3e-3
q = 2.9e-4
q = 0.015
Expression (RMA)
Hours of nickel exposure
J
DHRS3
Retinaldehyde
Retinol
ALDH1A1
RA
CYP26B1
clearance

Figure S7, related to Figure 7. A-B. Flow cytometric analysis of human Th9 cells cultured in the presence of RA vs. vehicle control. A. Representative plots of IL-9 expression in human Th9 cells differentiated with vehicle control or RA. B. Bar graph summarizing IL-9 expression in Th9 cells cultured with vehicle control or RA (n=4). Pooled data shown as mean + SEM; RA = 1000 nM; *p<0.05,**p<0.01,***p<0.005,****p<0.001, unpaired t-test. **C-E. Effect of house dust mite extract (HDM) on RA-regulated genes in $CD4^+$ T cells from healthy (black) or atopic (red) patients (original data from GSE73482).** C. Cumulative distributions indicate that HDM has a significantly greater effect on RA-regulated gene expression in atopic (red) than healthy samples (black), as evaluated by the Kolmogorov-Smirnov test. RA-regulated genes (n=645) are defined in Fig 1B. D. Gene set enrichment analysis (GSEA) in atopic $CD4^+$ cells finds that HDM significantly represses RA-induced genes (top bar, white) and induces RA-repressed genes (bottom bar, black). GSEA p-value is shown above the corresponding enrichment score. E. HDM's effect on representative RA-repressed (*IL9, IL13*) and RA-induced (*CCR9, NRIP1*) genes. Each point represents a single patient. Black bars represent mean values. Significance evaluated with FDR-adjusted p-values from paired t-tests. **F-J. Effect of nickel on RA-regulated genes in healthy (black) or nickel-allergic (red) skin (original data from GDS2935).** F. Cumulative distributions indicate that nickel exposure has a significantly greater effect on RA-regulated genes (n=665) in atopic (red) than healthy (black) samples, as evaluated by the Kolmogorov-Smirnov test G. GSEA in nickel-allergic skin samples finds that nickel exposure significantly induces RA-repressed genes (bottom bar), but does not significantly affect RA-induced genes (top bar). H,I. The effect of nickel exposure on representative genes regulated by RA (*IL9, NRIP1*) or involved in RA metabolism (*ALDH1A1, CYP26NB1, DHRS3*) in healthy (black) vs nickel-allergic (red) skin. Significance evaluated with FDR-adjusted p-values from 2-way ANOVA. J. Diagram of RA metabolism illustrating steps upregulated (red) or downregulated (blue) in atopic patients.

Table S2, primer list. Related to STAR Methods (Immunoprecipitation, Library preparation, and Chip-qPCR; Chromatin Conformational Capture (3C)).

Primer	Sequence
Il9 promoter forward primer (ChIP)	TTCAAACCGGGAAAAACCCT
Il9 promoter reverse primer (ChIP)	GTGACCCCTTCATTACCACC
Il9 E1 forward primer (ChIP)	ATGCAAATGACCCACAGGAA
Il9 E1 reverse primer (ChIP)	TGCGGAATGGGTTTTCACTT
Il9 E2 forward primer (ChIP)	ACAGGTCAGATGGAATGGGA
Il9 E2 reverse primer (ChIP)	ATCACCAGAGATAGACCCCC
Il9 E3 forward primer (ChIP)	GATCTGTTTCTGGCACCCAA
Il9 E3 reverse primer (ChIP)	GGGAAGGTTGCTCTGACAAT
Il9 DS forward primer (ChIP)	GCCTGGGTTTCTATTGCTCG
Il9 DS reverse primer (ChIP)	CTCATTCAGGATCGCAGGGA
Kynu promoter forward primer (ChIP)	GATTCAACAGGGTGGGAGGA
Kynu promoter reverse primer (ChIP)	TCCCCAAAGGACTGTACCCTAT
Sh3bp4 promoter forward primer (ChIP)	CACAGGACAAGAGAACCGC
Sh3bp4 promoter reverse primer (ChIP)	GGGATAGGGTGCGCCG
Ccr9 RARE forward primer (ChIP)	ACCCTTAACCCCCAGTTTCT
Ccr9 RARE reverse primer (ChIP)	TTCCGTGCCCGGAGAATTA
Negative control/gene desert forward primer (ChIP)	AGCTTCCATGCTTGTGGATG
Negative control/gene desert reverse primer (ChIP)	AGGATGTGGTGGGGTAGGTAA
3C probe for *Il9* locus (5'FAM-3'BHQ)	TGCCAGGAAATACCATTCCTCAGAA
3C anchor for *Il9* locus	GTCACTTGACAAAGGCTGTCT
3C variable region 1 (+6000bp from *Il9* anchor)	CTGATGATTCTTGTGGCCATG
3C variable region 2 (+16000bp from *Il9* anchor)	AATTCTCTACTTCCACCCCATG
3C variable region 3 (+19000bp from *Il9* anchor)	AGGATCTGAATGTGTGTTGGG
3C variable region 4 (+21500bp from *Il9* anchor)	CTTACAGTGTAGGCAAGTCGT
3C variable region 5 (+25000bp from *Il9* anchor)	GGGCGTCATACTCTTATCCATG
3C variable region 6 (+28000bp from *Il9* anchor)	ATGCATGTATCAAACCCTGGC
3C probe for *Fbxl21* normalization locus (5'FAM-3'BHQ)	ACCTCCCACCTTCTCTGTTCCTCAA
3C anchor for *Fbxl21* normalization locus	AGTAACACTGGTAGCATCCG
3C variable region for *Fbxl21* normalization locus	CTTTCTCACTGGGCAGAGAA

Table S3, luciferase constructs. Related to STAR Methods (Luciferase detection)

Luciferase construct containing Il9 promoter fragment

CTCGAGCAGTGAGTTGAGCCCCCTTTGCCATCCTCCAGCAGATGACTCTCCCCAGTCCCCTAAATCTACCTTCAGATT
TTCAATAAGGTAATTGGTGTCTCTGATGCCCCATGTGGTGCTGCATCTCTGGCCCAGCACAGAACTGAAGAGCAAAA
CAGAGGCAAGGATGTATGTCACCAACATGTTGACGGGAGTCTGGAACTCAGTCTACCAGCATCTTCCAGTCTAGCTG
TATTTAAAGCTCTTCAAACCGGGAAAAACCCTGACATCAAACTGATACCCAGTGCCCACTTTTTTCTCTGTAAGTTGAG
GCCAATTGAGATATTGAAAAAAAAATCAGTCTGAGTCACTTGACAAAGGCTGTCTTA*TGCCAGGAA*ATACCA**TTCCTC**
AGAAAAGATGCTCTTCAAATAGTCGGGTTCTGAAATACTAAAGGAAAAGTTAAAGATCTAGCCCCAACCCCCTTTAAA
AGCAGGAATTCTGGTTGTGAGAATCAAAACACTTTCCATGAAAGCCCAGGTCTGTGTTTTCCCCTCCACATTAGTGAG
AAATGCTGATAGACAGTGAGTTACAGGGGTGGTAATG**AAGGGGTCAC**ACTGGGGATATCAGGGGAAAGCAAGACTT
GCCTTTCACTCATTGGGGTTTTCCTCTGGCTATTGGAGCCTCAGTTTACTTGATTGCTAGATACTCACAGTATGTCAG
GCCTAGGAACAAAAGTTCTACCTCGTACATACACCTCTGAGAAGTCGCTCTATGCGAGTATATGAGTTGTTTTCTGTA
AGTACGTGGATGCTGGAACTGTGCTTGCTAGCATTGGCCTTGAGGA*TCCTTGGAA*TCAAGCTT

Luciferase construct containing Il9 promoter fragment + E1 fragment

GGTACCTTAAGAAGCTGAACATGGAAGCATTTGAGGAGTGAGGAGATGACTTGGGGAG**CTGAGCCCTT**GGTGCAGG
GCTTGCTCTCATCATGAAGGCTGCAGGAGGAAGGGTTGTGGGACAGGGACTCCCA**TCCTGTCCCC**ACAGACCCACA
CACTCACTTATGCAAAACAAGCAGGGTAAGGACTAGGAGGAGAGCACTGCAACTGAGCACACCATTGAGGCAACAA
GCGCTGTCCAAGCCCTGTGTGACTTTCGAAGCTAGGC*TTCTAGGAT*TT*TTCTCAGCA*TCAGACTGCAAGTATGCAAAT
GACCCACAGGAAATACGCCCAACTTCAAAATGACTCACTGACATTACC*TACAGGGGAA*GCTGGGGAGCTGAACGCA
GGCCAAGAACGAGTGCAGATACTATCTTTTGCAATAAATGACAGGGGACAATAATCAACCATTTATTTTG*TTCCAAAGA*
TAAAGCTCCACACACTTAGTTTGTGATTAAAAGCCTAGTGTGTCATAGATTATTTCTACAACAAAATGGCTATTTG**TTCT**
AGGAAGTCACAACACAAAATGACCCCCAAAATTTTTTTCTTAAATAGCTAAAT*TTCCAAGTGAA*AACCCATTCCGCATT
TTACTCTATAAACAGTGGAGAGATAACTAG**TTCCAAGAA**TCCTTCAGCACTAATTTCTTTGTCAAGTAGTTACTTAGAC
CAGTATTTCTCATCAGCTATCTGGGGGTAAACCCCCCTGGATACACTT*TTCTCCAAA*GGAGGAT**GCTTTTGAGCT**GGA
CACCATGGCCTGC*TCCCCAGAA*TCTCTCCTAAGCCCATTCTTCTTTGCCTGATGCTGGGATGCTGTTCCCCTCGAGC
AGTGAGTTGAGCCCCCTTTGCCATCCTCCAGCAGATGACTCTCCCCAGTCCCCTAAATCTACCTTCAGATTTTCAATA
AGGTAATTGGTGTCTCTGATGCCCCATGTGGTGCTGCATCTCTGGCCCAGCACAGAACTGAAGAGCAAAACAGAGGC
AAGGATGTATGTCACCAACATGTTGACGGGAGTCTGGAACTCAGTCTACCAGCATCTTCCAGTCTAGCTGTATTTAAA
GCTCTTCAAACCGGGAAAAACCCTGACATCAAACTGATACCCAGTGCCCACTTTTTTCTCTGTAAGTTGAGGCCAATT
GAGATATTGAAAAAAAAATCAGTCTGAGTCACTTGACAAAGGCTGTCTTA*TGCCAGGAA*ATACCA**TTCCTCAGAA**AAG
ATGCTCTTCAAATAGTCGGGTTCTGAAATACTAAAGGAAAAGTTAAAGATCTAGCCCCAACCCCCTTTAAAAGCAGGA
ATTCTGGTTGTGAGAATCAAAACACTTTCCATGAAAGCCCAGGTCTGTGTTTTCCCCTCCACATTAGTGAGAAATGCT
GATAGACAGTGAGTTACAGGGGTGGTAATG**AAGGGGTCAC**ACTGGGGATATCAGGGGAAAGCAAGACTTGCCTTTC
ACTCATTGGGGTTTTCCTCTGGCTATTGGAGCCTCAGTTTACTTGATTGCTAGATACTCACAGTATGTCAGGCCTAGG
AACAAAAGTTCTACCTCGTACATACACCTCTGAGAAGTCGCTCTATGCGAGTATATGAGTTGTTTTCTGTAAGTACGTG
GATGCTGGAACTGTGCTTGCTAGCATTGGCCTTGAGGA*TCCTTGGAA*TCAAGCTT

Luciferase construct containing Il9 promoter fragment + E2 fragment

GGCCTAACTGGCCGGTACCTCCAGGATTTTGCTTCA*TTGTTGGAA*ATTGGGGGGTCTATCTCTGGTGATACCCTCAC
CACATCCAGCACACCTGAGACATAATGCGTACTCTCCAGCAAAGGTCTGGCTCACCCCGACTGCACACTTCAGTGTG
TGCCTGCAAAAATGATAGTGTTTTCCAGCTTGAT*TTCAGAAAA*TGATAGGCAAAGCAGAGAGAGAGAGTCACCCCGTC
TGTGTGATGTTCAGTAAGAGGTAGATGGCGGATCCCCTGGAGTGCTCGTACATGC*TTCTCAGTA*ACCACGGGGACTC
TCCAGTGGCCAGGACTTCCTATTACAGTCGGCTGCTGGAGTTTCATTTTGGCTCAAAGAGCACAGTATTCGCTGTC**TT**
CCTTGAAAATGGTGGCG*TGCGTTTGTGAA*TTTTCTTTGCCAGGGGTCCTCTTTGGTCAACTGAGTTTATTTAT**GATCT**
GGAGAAAGTAGTCCCTAGTGTCT**TTCTAGGAA**AAGTCAACACTCTGGGTGAGTGTCTGTCTGGGTTAGGATCTGAAT
GTGTGTTGGGATCTTGTTCTAATCAGA***TCTTCCAGAAAC***CATTTGA*TTCAGCTGAG*CACTGTCTGTCTGGAAACTTGCT
ATCTCCTGGACTCCAG*TTCACTGCA*CATTCCGGTCTCAAATGCAACCTCATTTCTGTGGGCTCTGAGGTGCCTTCAGG
ATTTAGTGTACTTACAATGGGTTGTCCTAGGTCAGGTAGTGATACCTGAGGTAGTCCTGATCTTTCTGGCATGACTTA
AAGCTCGAGCAGTGAGTTGAGCCCCCTTTGCCATCCTCCAGCAGATGACTCTCCCCAGTCCCCTAAATCTACCTTCA
GATTTTCAATAAGGTAATTGGTGTCTCTGATGCCCCATGTGGTGCTGCATCTCTGGCCCAGCACAGAACTGAAGAGC
AAAACAGAGGCAAGGATGTATGTCACCAACATGTTGACGGGAGTCTGGAACTCAGTCTACCAGCATCTTCCAGTCTA
GCTGTATTTAAAGCTCTTCAAACCGGGAAAAACCCTGACATCAAACTGATACCCAGTGCCCACTTTTTTCTCTGTAAGT
TGAGGCCAATTGAGATATTGAAAAAAAAATCAGTCTGAGTCACTTGACAAAGGCTGTCTTA*TGCCAGGAA*ATACCA**TT**
CCTCAGAAAAGATGCTCTTCAAATAGTCGGGTTCTGAAATACTAAAGGAAAAGTTAAAGATCTAGCCCCAACCCCCTT
TAAAAGCAGGAATTCTGGTTGTGAGAATCAAAACACTTTCCATGAAAGCCCAGGTCTGTGTTTTCCCCTCCACATTAG
TGAGAAATGCTGATAGACAGTGAGTTACAGGGGTGGTAATG**AAGGGGTCAC**ACTGGGGATATCAGGGGAAAGCAAG
ACTTGCCTTTCACTCATTGGGGTTTTCCTCTGGCTATTGGAGCCTCAGTTTACTTGATTGCTAGATACTCACAGTATGT

CAGGCCTAGGAACAAAAGTTCTACCTCGTACATACACCTCTGAGAAGTCGCTCTATGCGAGTATATGAGTTGTTTTCT
GTAAGTACGTGGATGCTGGAACTGTGCTTGCTAGCATTGGCCTTGAGGA*TCCTTGGAA*TCAAGCTT

Luciferase construct containing Il9 promoter fragment + E3 fragment

GGTACCTATAAAAGGATGGGCAAGCCAACTCTCAGCATGTGTTTATATCTGTAAAGAATCACTGGACGTATTGCTTGT
CATGACTGAATTTAAAACTAGAAAATGGCAAGTTTTAAAGTGGTCGCCTGCTTTGACAAAGCTATGCAAAACACACTCT
TTTAGTGATCTGTTTCTGGCACCCAAACATTTTTTTTTGTCTCAGCACAAGTCTTCTGCATCCTGTTTGTGGTTTGAAAG
GAAAAAAATCTGATCAGAGAGACTGATACAGCTCATACTAAATGATTGTCAGAGCAACCTTCCCACCTCCTCCTCCTC
CTTCTCAAACATTCGAGTTTGTAAAAACTCTATTCACTGTGTCACTAAACCCACCGAGTGCCCACACTTTCACATGATT
TGCCCCAACATGGAACCTCTGAAAATCTGCTGTCTACACCGCCATAGACCTGTCATAAGCAG**TTCATGGAA**TTGGCA
TGATGAGGACTGGTATCAAGAGTCACTAT**CTTCTGTTAC**CTCATTCACTCCTAATCTTCAAGCCCCTGTGGTCTGAGG
TTTCTCTTGCAGTTTCTTTTGTTCAGTTTAAGAAAAAACAGCTGCTTGGCAGACAAGCCTCATGACATCCTTTGAAGTC
TTGTAAGATACTCGTTAGCAAATTATAAGGTCTGCTAAACAAAGGAAAAACCTCGAGCAGTGAGTTGAGCCCCCTTTG
CCATCCTCCAGCAGATGACTCTCCCCAGTCCCCTAAATCTACCTTCAGATTTTCAATAAGGTAATTGGTGTCTCTGATG
CCCCATGTGGTGCTGCATCTCTGGCCCAGCACAGAACTGAAGAGCAAAACAGAGGCAAGGATGTATGTCACCAACAT
GTTGACGGGAGTCTGGAACTCAGTCTACCAGCATCTTCCAGTCTAGCTGTATTTAAAGCTCTTCAAACCGGGAAAAAC
CCTGACATCAAACTGATACCCAGTGCCCACTTTTTTCTCTGTAAGTTGAGGCCAATTGAGATATTGAAAAAAAAATCAG
TCTGAGTCACTTGACAAAGGCTGTCTTA*TGCCAGGAA*ATACCA**TTCCTCAGAA**AAGATGCTCTTCAAATAGTCGGGTT
CTGAAATACTAAAGGAAAAGTTAAAGATCTAGCCCCAACCCCCTTTAAAAGCAGGAATTCTGGTTGTGAGAATCAAAA
CACTTTCCATGAAAGCCCAGGTCTGTGTTTTCCCCTCCACATTAGTGAGAAATGCTGATAGACAGTGAGTTACAGGGG
TGGTAATG**AAGGGGTCAC**ACTGGGGATATCAGGGGAAAGCAAGACTTGCCTTTCACTCATTGGGGTTTTCCTCTGGC
TATTGGAGCCTCAGTTTACTTGATTGCTAGATACTCACAGTATGTCAGGCCTAGGAACAAAAGTTCTACCTCGTACATA
CACCTCTGAGAAGTCGCTCTATGCGAGTATATGAGTTGTTTTCTGTAAGTACGTGGATGCTGGAACTGTGCTTGCTAG
CATTGGCCTTGAGGA*TCCTTGGAA*TCAAGCTT

Consensus gamma interferon activation site (GAS) that binds to STAT5

Half GAS